1-1-2019

Drainage and Sedimentary Responses to Dynamic Topography

Xuesong Ding

Tristan Salles

Nicolas Flament
University of Wollongong, nflament@uow.edu.au

Claire Mallard

Patrice F. Rey

Drainage and Sedimentary Responses to Dynamic Topography

Abstract

Dynamic topography due to mantle flow contributes to shaping Earth's evolving landscapes by affecting sediment routing, which has rarely been explored in source-to-sink contexts. Here we design a generic model to investigate the impact of dynamic topography on both landscape evolution and stratigraphic formations. An imposed wave of dynamic topography propagates laterally under a fixed continent, exerting transient surface uplift and subsidence. We find that a migrating dynamic topography can induce significant drainage reorganizations and affect sediment routing from source to sink. Variations in sediment supply driven by the lateral migrating dynamic topography contribute to the formation of diachronous unconformities along the margin. The predicted sediment flux histories are then put into perspective with the Cretaceous sedimentary records along the Southern African margins. Finally, we demonstrate that correlating offshore depositional hiatuses and unconformities has the potential to constrain the spatiotemporal evolution of past dynamic topography events.

Publication Details

Ding, X., Salles, T., Flament, N., Mallard, C. & Rey, P. F. (2019). Drainage and Sedimentary Responses to Dynamic Topography. Geophysical Research Letters, Online First 1-10.

Geophysical Research Letters

RESEARCH LETTER
10.1029/2019GL084400

Drainage and Sedimentary Responses to Dynamic Topography

Xuesong Ding[1,2], Tristan Salles[1], Nicolas Flament[3], Claire Mallard[1], and Patrice F. Rey[1]

[1]Basin GENESIS Hub, EarthByte Group, School of Geosciences, The University of Sydney, Sydney, NSW, Australia, [2]Now at Department of Earth, Planetary and Space Sciences, University of California, Los Angeles, CA, USA, [3]School of Earth, Atmospheric and Life Sciences, University of Wollongong, Wollongong, NSW, Australia

Key Points:
- A propagating wave of dynamic topography can induce significant drainage reorganizations and affect sediment routing from source to sink
- Variations in sediment supply driven by the migration of dynamic topography can create diachronous unconformities along continental margins
- Our model predicts sediment flux histories comparable to that along the Southern African margins during Cretaceous times

Supporting Information:
- Supporting Information S1

Correspondence to:
X. Ding,
xuesong.ding@sydney.edu.au;
xuesong.ding@epss.ucla.edu

Citation:
Ding, X., Salles, T., Flament, N., Mallard, C., & Rey, P. F. (2019). Drainage and sedimentary responses to dynamic topography. *Geophysical Research Letters*, *46*. https://doi.org/10.1029/2019GL084400

Received 2 JUL 2019
Accepted 2 DEC 2019
Accepted article online 9 DEC 2019

Abstract Dynamic topography due to mantle flow contributes to shaping Earth's evolving landscapes by affecting sediment routing, which has rarely been explored in source-to-sink contexts. Here we design a generic model to investigate the impact of dynamic topography on both landscape evolution and stratigraphic formations. An imposed wave of dynamic topography propagates laterally under a fixed continent, exerting transient surface uplift and subsidence. We find that a migrating dynamic topography can induce significant drainage reorganizations and affect sediment routing from source to sink. Variations in sediment supply driven by the lateral migrating dynamic topography contribute to the formation of diachronous unconformities along the margin. The predicted sediment flux histories are then put into perspective with the Cretaceous sedimentary records along the Southern African margins. Finally, we demonstrate that correlating offshore depositional hiatuses and unconformities has the potential to constrain the spatiotemporal evolution of past dynamic topography events.

Plain Language Summary Convective motion within Earth's interior result in transient uplift and subsidence of the surface is called *dynamic topography*. This process slowly shapes landscapes over millions of years and identifying its fingerprints in the rock record remains a challenge. This study uses numerical modeling to investigate the erosional and depositional response of landscapes to sea level change and to mantle flow. We show that unlike sea level change, dynamic topography reorganizes river flows and changes sediment supply to offshore regions, generating various stratal patterns. We model a simple circular landscape that evolves similarly to the southern African landscape between 140 and 66 million years ago and suggest sedimentary fingerprints to link the evolution of the Earth's surface to the dynamics of its deep interior.

1. Introduction

Deep Earth processes play a significant role in shaping Earth's evolving landscapes by imposing transient episodes of dynamic topography (Braun, 2010; Flament et al., 2013). Examples of landscapes that have recorded dynamic topography include the Colorado Plateau (Braun et al., 2013; Karlstrom et al., 2012; Liu & Gurnis, 2010; Moucha et al., 2009), the Iceland Plateau (Bijwaard & Spakman, 1999; Maclennan et al., 2001), the South African Plateau (Braun et al., 2014; Flament et al., 2014; Gurnis et al., 2000; Moucha & Forte, 2011), and the Australian continent (Czarnota et al., 2013, 2014; Matthews et al., 2011; Sandiford, 2007). Field observations and numerical investigations suggest that interactions between dynamic topography and surface processes can be preserved in the geological record (Braun et al., 2013; Burgess et al., 1997; Burgess & Moresi, 1999). For example, dynamic uplift can induce stratal unconformities in offshore regions (Champion et al., 2008; Rudge et al., 2008), while dynamic subsidence can explain exceedingly thick sediment accumulation in depositional basins (Downey & Gurnis, 2009). However, it remains challenging to isolate the fingerprints of dynamic topography in the sedimentary record that primarily reflects shallower tectonic processes (Eakin & Lithgow-Bertelloni, 2018). Even in tectonically stable regions, external factors, such as climate or eustasy, can potentially produce geomorphologic and stratigraphic patterns that interfere with those of dynamic topography.

Large-scale and long-term landscape evolution modeling (LEM) is useful to evaluate the landscape and drainage responses to dynamic topography (Braun et al., 2013; Ruetenik et al., 2016; Salles et al., 2017). However, most LEMs do not explicitly predict stratigraphic architectures, making it difficult to explore the sedimentary responses to dynamic topography. Stratigraphic forward modeling enables to investigate the

stratigraphic signatures of sea level changes and tectonics but usually assumes constant sediment supply from the source region. The landscape evolution model *pyBadlands* simulates geomorphic processes and stratigraphic formations in a combined source-to-sink system (Chang & Liu, 2019; Ding et al., 2019; Salles et al., 2018; Salles & Hardiman, 2016). Comparing with most LEMs and stratigraphic forward modelings, it provides a more realistic approach of representing sediment supply and sediment routing systems. Here we use *pyBadlands* to explore the erosional and depositional landscape evolution in response to both sea level change and dynamic topography. Our results show that dynamic topography can induce significant drainage reorganizations and affect the long-term (~10s Myr) evolution of drainage systems. Dynamic topography also has distinct impacts on the formation of second- (10–80 Myr) and third-order (1–10 Myr) stratigraphic cycles (Vail et al., 1977), depending on its migrating direction relative to the sediment transport direction.

2. Numerical Experiments

We consider a model of circular continent 700 km in diameter with a spatial resolution of 1 km (Figure 1a). Its initial landscape consists of a central plateau (source area) surrounded by an alluvial plain (transfer zone) and a continental margin (sink area). As forcing factors driving landscape evolution and stratigraphic formations, we impose rainfall, eustatic sea level, and a westward propagating wave of dynamic topography. For simplicity, other tectonic inputs (e.g., flexure and thermal subsidence) are not considered. The circular geometry of the continent makes it possible to investigate the responses of river systems with varying sediment transport directions relative to the wave of dynamic topography. In *pyBadlands*, erosion, sediment transport and deposition are described using both fluvial and hillslope processes (Salles et al., 2018; Salles & Hardiman, 2016). The governing equations and model parameters are provided in the supporting information.

We compare three cases forced with a uniform precipitation rate of 1.0 m/year (see Table S1 in the supporting information). Case 1 is a reference experiment in which the landscape evolves under a constant eustatic sea level (0 m). Case 2 involves a periodic eustatic sea level curve with fluctuations of 50 m every 5 Myr (Figure S1b) comparable to million-year scale eustatic change (Miller et al., 2005). Case 3 considers a sinusoidal wave of positive dynamic topography with a wavelength of 1,000 km and amplitude of 300 m propagating to the west at 5 cm/year (Figure 1a). The average rate of the surface uplift or subsidence is 30 m/Myr, which is comparable to the inferred dynamic tilting rate of northern Australia (5 to 75 m/Myr; Czarnota et al., 2013). It takes 34 Myr for this dynamic topography wave to travel across the whole model domain. We run all experiments for 36 Myr with an output interval of 300 kyr, recording 120 stratigraphic layers.

3. Results

3.1. Evolution of Landscapes and Drainage Networks

In the absence of dynamic topography forcing, the drainage pattern in Cases 1 and 2 remains radial with the central plateau and the alluvial plain symmetrically eroded (Figures S1a and S1b). Sediments accumulate in deltas homogeneously distributed along the continental margin (Figure S1a and S1b). In Case 2, periodic eustatic sea level changes do not affect this pattern (Figure 1f) but add cyclical fluctuations with increasing fluvial erosion and offshore sedimentation during periods of falling eustatic sea level (Figures 1g and 1h).

In Case 3, rivers with opposite sediment transport directions respond differently to the westward propagating dynamic topography, which results in complex drainage reorganizations. On the east side of the domain, the dynamic uplift propagates upstream creating a coastal bulge that diverts river flows (e.g., R2 in Figure 1 b). The river mouth of R2 migrates along the southern margin in the same direction as the dynamic topography from 3.6 to 10 Myr, with a slightly higher migrating rate (~5.5 cm/year) than that of dynamic topography (5 cm/year). The coastal bulge is incised by small east directed rivers carrying limited sediments to the coast (e.g., R1 in Figure 1b). The eastern margin eventually subsides from 11.7 Myr, and its accumulative subsidence allows some diverted inland rivers to breach the coastal bulge and join those small rivers from 12.6 Myr (e.g., R1′ in Figure 1c), whereas other diverted rivers on the northern and southern plains retain their courses (e.g., R2′ in Figure 1c). On the west side of the domain, the surface slope is steepened westwards by the propagating uplift from 7 to 17 Myr, which stimulates the incision of the western side of the plateau (Figures 1b and 1c). It also exposes the western margin, leading to an increasingly narrower continental

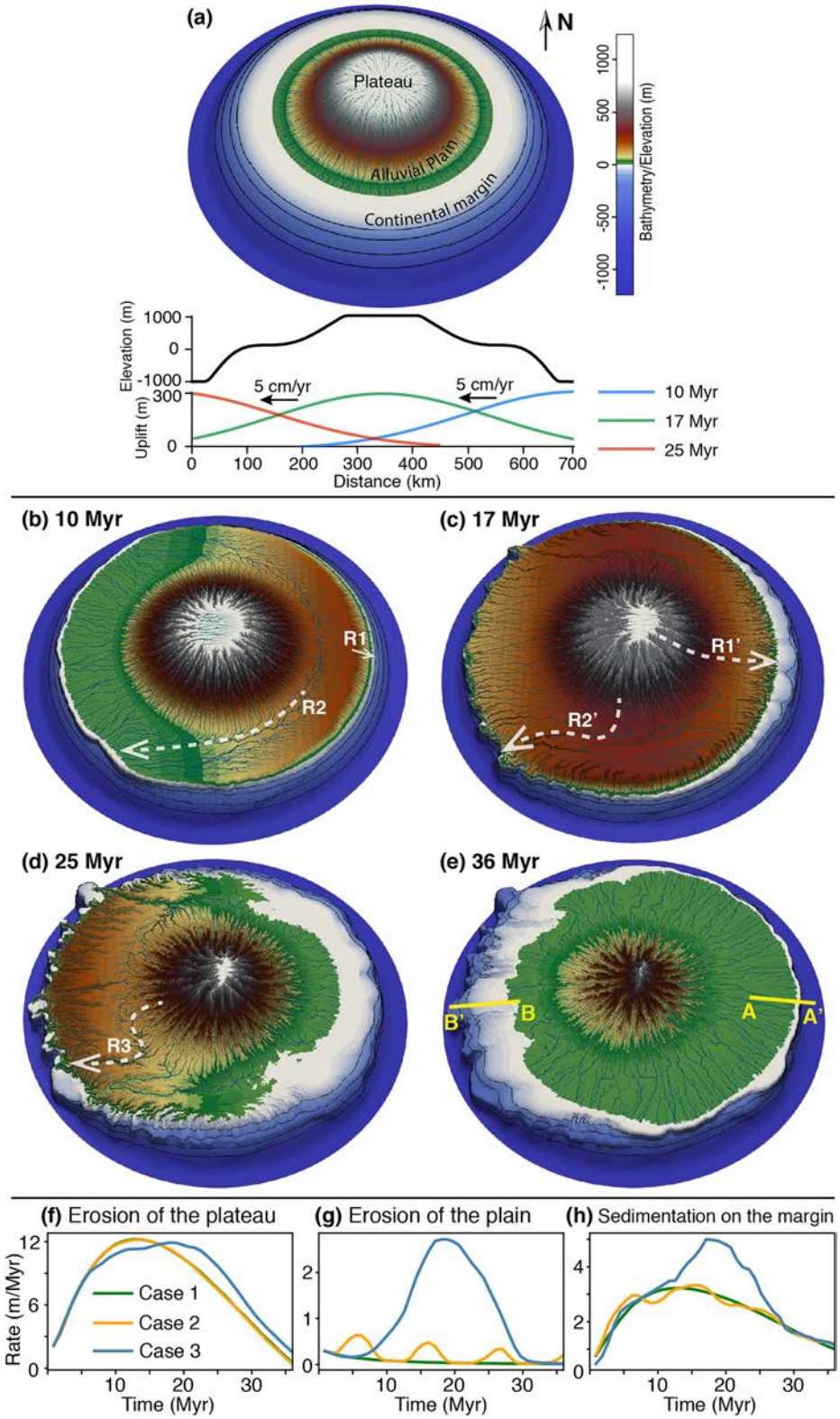

Figure 1. (a) Initial surface of a circular continent under which a wave of dynamic topography propagates at 5 cm/year. The surface uplift induced by the migrating dynamic topography is shown at 10, 17, and 25 Myr. Note the different vertical scales for the topography profile and uplift profiles. (b–e) Snapshots of the landscape and river network evolution for Case 3, at 10, 17, 25, and 36 Myr. Dashed arrows indicate significant drainage reorganization events of rivers R1 to R3. A-A′ and B-B′ indicate the locations of the cross sections shown in Figure 2. Average erosion rate of (f) the plateau and (g) the whole alluvial plain and (h) average sedimentation rate over the whole continental margin are shown for Cases 1–3.

shelf (Figures 1c and 1d). From 21 to 29 Myr, as dynamic subsidence propagates downstream to the west, the slope of the alluvial plain is reversed and rivers are rerouted (e.g., R3 in Figure 1d). At 36 Myr, the progressive subsidence of the western margin leads to significant flooding of the plain and eventually to a broader shelf compared to that of the eastern margin (Figure 1e). In summary, the migrating dynamic topography affects all segments of the source-to-sink system, with most significant impacts on increasing the fluvial erosion and offshore sedimentation (Figures 1f–1h).

3.2. Formation of Stratigraphic Architectures

We document the stratal stacking patterns along one section for Cases 1 and 2 (C1-C1′ in Figure S1a and C2-C2′ in Figure S1b) and two sections for Case 3 (A-A′ and B-B′ in Figure 1e). On these cross sections, stratigraphic layers are displayed with a time interval of 0.9 Myr. We also reconstruct both the sediment supply and the erosion of strata (in km^2/Myr) on each cross section by calculating the volume of sediments deposited and eroded across a unit width in 0.9-Myr increments. To understand how the two margins in Case 3 are different in terms of the timing of deposition and unconformity formation, we build Wheeler diagrams (i.e., chronostratigraphic diagram) along the two sections (see Text S2 in the supporting information).

In Case 1, the average sediment supply is 0.87 km^2/Myr, with fluctuations induced by shifts of the river mouth relative to cross section C1-C1′ (Figure S1c). The stratal stacking pattern on C1-C1′ shows an overall progradational depositional trend, during which sediments bypass the shelf without erosion (Figure S1e). Sediment accumulates predominantly into offshore and deep marine deposits, with little alluvial deposit. In Case 2, the average sediment supply is 0.83 km^2/Myr, with fluctuations that are consistent with the eustatic cycles (Figure S1d). Episodes of strata erosion between 0 and 4.8, 10 and 15, 21 and 24.9, and 31 and 33.3 Myr correspond to eustatic sea level fall (forced regression; Figure S1d). The strata stacking pattern reveals sequence cycles bounded by four subaerial unconformities at 4.8, 15, 24.9, and 33.3 Myr (red lines in Figure S1f). Eustatic fluctuations also lead to increased alluvial deposition and to periodic variations in shoreface and distal offshore sedimentation.

In Case 3, the eastern margin undergoes uplift from 1.8 to 11.7 Myr and subsidence from 11.7 to 22.5 Myr. Sediment transport to the eastern margin occurs in the direction opposite to the westward propagating dynamic topography, resulting in low sediment supply (0.725 km^2/Myr on average). Sediment supply is low (<0.7 km^2/Myr) between 3 and 11.7 Myr (Figure 2a) because the margin is exposed by dynamic uplift and rivers are rerouted (e.g., R1 in Figure 1b). A degradational stacking pattern (D or falling-stage systems tract FSST) develops due to the dynamic uplift, during which sediments deposited before 8.4 Myr are totally eroded, and only a fraction of sediments deposited between 8.4 and 11.7 Myr are preserved (Figures 2b–2d). The strata stacking trend changes to a "progradation to aggradation" pattern (PA or lowstand systems tract LST) from 11.7 Myr when the margin starts to subside, with sediments onlapping onto the erosional basal unconformity (red lines in Figures 2b and 2c). Strata regression peaks at 13.5 Myr, after which strata stacking follows a retrogradational pattern (R or transgressive systems tract TST). Sediments continue onlapping onto the basal unconformity, with dominant accumulation of coastal plain and shoreface facies (Figures 2b–2d). Subsidence of the eastern margin also enables diverted rivers to breach the coastal bulge from 13.2 Myr (e.g., R1′ in Figure 1c). Sediment supply to the eastern margin then significantly increases to 2.5 km^2/Myr and remains large as the margin subsides (Figure 2a). Stratal stacking then shifts to an "aggradation to progradation" stacking pattern (AP or highstand systems tract HST) from 22.5 to 36 Myr (Figures 2b–2d).

The western margin in Case 3 undergoes uplift from 10 to 20 Myr and subsidence from 20 to 30 Myr. Sediment transport to the western margin occurs in the same direction as the westward propagating dynamic topography, resulting in a larger sediment supply (1.72 km^2/Myr on average). Changes in sediment supply before 10 Myr reflect changes in the location of the river mouth relative to cross section B-B′ (Figure 2e). During the uplift phase of the western margin, the stratal stacking trend changes from progradation (P or HST) to degradation (D or FSST) at 12 Myr and sediment supply increases up to 8.5 km^2/Myr at 19 Myr (Figures 2e–2h). From 20 to 24.3 Myr, the subsidence of the western margin induces river rerouting (e.g., R3 in Figure 1d), resulting in a sharp decrease in sediment supply to 0.3 km^2/Myr (Figure 2e). The propagating subsidence leads to a retrogradational pattern (R or TST) and accumulation of thick alluvial plain

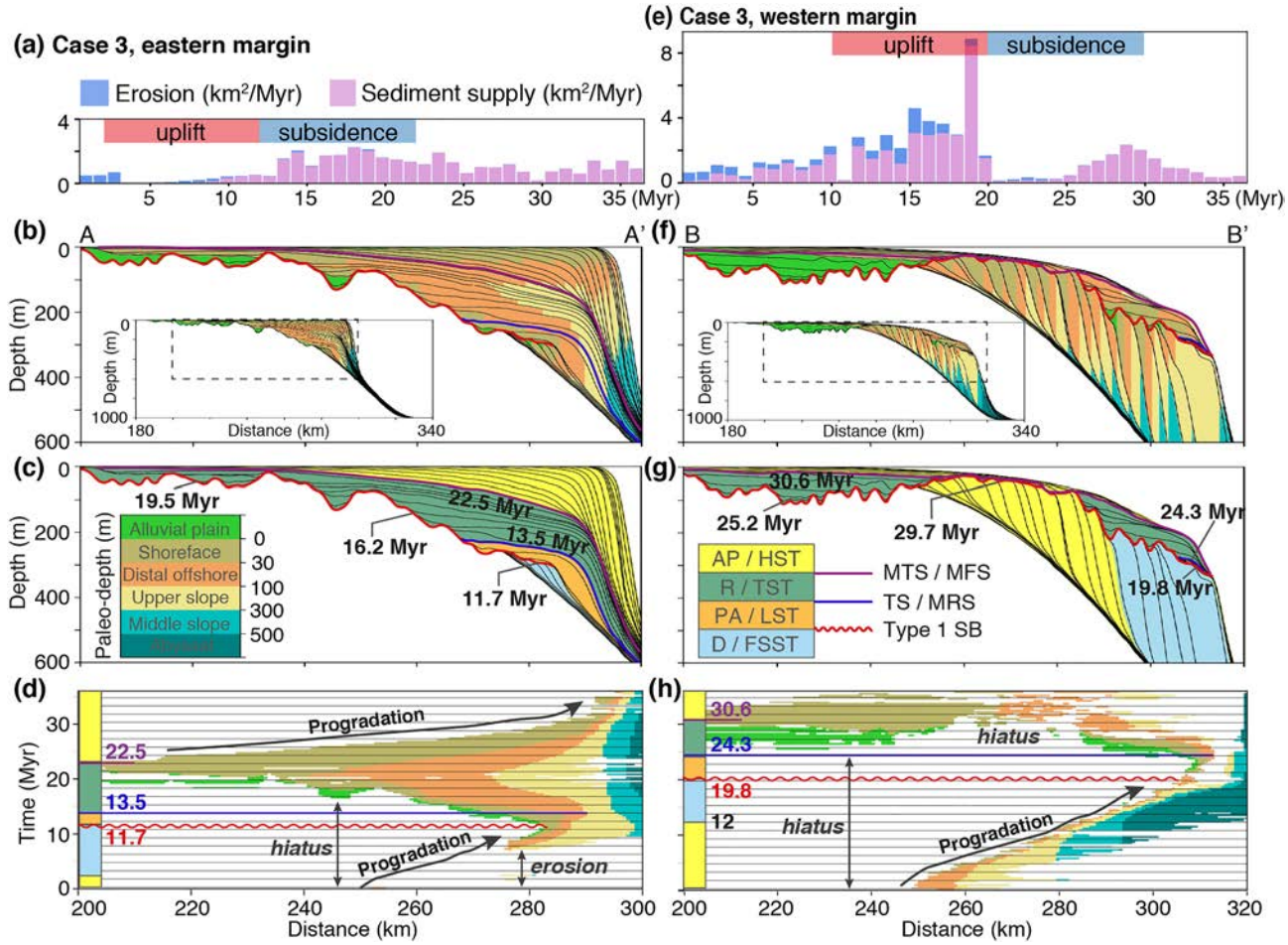

Figure 2. (a) Sediment supply histories and erosion of stratigraphic layers, stratal stacking patterns represented by (b) depositional environments, (c) interpreted systems tracts, and (d) Wheeler diagrams reconstructed for Case 3 on the eastern margin along A-A′. (e–h) Same for the western margin along B-B′. See Figure 1e for cross section locations. Paleo-depth is assumed to be a proxy for depositional environments, including alluvial plain (>0 m), shoreface (or delta front, 0–30 m), distal offshore (or prodelta, 30–100 m), upper slope (100–300 m), middle slope (300–500 m), and abyss (>500 m). Key stratigraphic surfaces and their timing are indicated in c, d, g, and h. Systems tracts are interpreted for Case 3 with abbreviations: A = aggradation, P = progradation, R = retrogradation, D = degradation, HST = highstand systems tract, TST = transgressive systems tract, LST = lowstand systems tract, FSST = falling-stage systems tract, MTS = maximum transgressive surface, MFS = maximum flooding surface, TS = transgressive surface, MRS = maximum regressive surface, and SB = sequence boundary (Hunt & Tucker, 1992; Neal & Abreu, 2009; Neal et al., 2016).

deposits on the proximal shelf from 25.2 Myr, and shoreface deposits on the distal shelf from 24.3 Myr and on the middle shelf only from 29.7 Myr (Figures 2f–2h). The stratal stacking trend changes to a progradational pattern (P or HST) from 30.6 to 36 Myr due to noncreation of accommodation (Figures 2f–2h) once the western margin is no longer affected by dynamic topography.

In summary, Case 3 shows that the propagating wave of dynamic topography induces distinct stratigraphic features not seen in Cases 1 (precipitation only) and 2 (precipitation and cyclical sea level changes). The wave of dynamic topography also results in different stratal geometries, formation of unconformities, and sediment accumulation patterns along the eastern and western margins. In particular, there is (1) more sediment supply during the uplift of the western margin from 10 to 20 Myr, (2) more sediment supply during the subsidence of the eastern margin from 13 to 23 Myr, (3) different shapes of unconformities, (4) more alluvial deposition on the western margin, and (5) more significant erosion of the coastal plain and shoreface deposits on the western margin. These differences are related to the angular relationship between the direction of migration of the dynamic topography and the direction of sediment transport and, therefore, constitute potential constraints on the migrating direction of dynamic topography.

4. Application to Southern Africa

Over the last two decades, high-resolution seismic data and thermochronology data have improved our understanding of the tectonic and geomorphic evolution of Southern Africa (Baby et al., 2018; Baby et al., 2018; Brown et al., 2002; Guillocheau et al., 2012; Said et al., 2015; Stanley et al., 2015; Tinker et al., 2008a). For example, Hu et al. (2018) recently proposed a lithospheric delamination model for the uplift history of southern Africa based on seismic observations and geodynamic modeling. In contrast, from sediment flux data and landscape evolution modeling Braun et al. (2014) suggested that Southern Africa migrated over a fixed mantle superwell during the Late Cretaceous. The models presented in Braun et al. (2014) reveal enhanced landscape erosion during continental tilting, resulting from the reorganization of drainage systems by increasing the drainage area. Our Case 3 also predicts increased erosion of the alluvial plain during the uplift phase of the migrating dynamic topography (Figure 1g). Furthermore, Case 3 predicts sediment flux histories and uplift-induced subaerial unconformities of three marginal basins (Southeast, South, and Southwest Basins; Figures 3a and 3b) that are comparable to those from the Southern Mozambique Basin, the Outeniqua Basin, and the Orange Basin of southern Africa (Figures 3c and 3d). Note that Case 3 is not specifically designed to reconstruct the topographic evolution of southern Africa. Given the simplicity of the model set up, we compare the trends of changes in sediment flux and their relationship with the formation of subaerial unconformities rather than the exact timing and amplitudes of the changing sediment flux.

Based on the drainage and sedimentary evolution in Case 3, it is possible to propose that the Southern African landscape was shaped by migration of the plate over a mantle superwell during Cretaceous times. The low sediment flux to the Southern Mozambique Basin before 113 Ma (Figure 3d), similar to the low sediment flux to the Southeast basin from 5 to 12 Myr (Figure 3b), could have been induced by dynamic uplift that would have prevented rivers from draining eastwards (e.g., R1 and R2 in Figure 1b). Diverted rivers would instead have fed the Outeniqua Basin and the Orange Basin (e.g., R2 in Figure 1b), explaining their large sediment flux over the same period (Figures 3b and 3d). From 113 to 92 Ma, the enhanced sediment flux to the Southern Mozambique Basin could have been induced by the rejuvenation of diverted rivers that would have resumed draining eastwards (e.g., R1′ in Figures 1c and 3d). As a result, the sediment flux to the Outeniqua Basin and the Orange Basin would have been reduced during that period (Figures 3b and 3d). In the Southern Mozambique Basin, an erosional unconformity (92 Ma) and well-defined forced regression wedges indicate marginal uplift at around 95–90 Ma as well as the termination of the uplift (Braun et al., 2014). The significantly increased sediment flux to the Southern Mozambique Basin is similar to that induced by the dynamic subsidence applied in our model (Figures 3b and 3d). Two stratal unconformities are documented for the Outeniqua and Orange Basins (Guillocheau et al., 2012; Tinker et al., 2008b). Our model suggests that the uplift of the Outeniqua Basin at 76 Ma and the uplift of the Orange Basin at 66 Ma could reflect the westward migration of dynamic uplift. Furthermore, the propagating uplift across the source region would have been consistent with the enhanced sediment flux to the Outeniqua Basin between 92 and 76 Ma and to the Orange Basin between 92 and 66 Ma (Figures 3b and 3d).

Braun et al. (2014) suggested that the mean erosion rate of the Southern Africa plateau could have been 100 m/Myr, which is much larger than the predicted average erosion rate (~12 m/Myr) of the central plateau for Case 3. The difference could be due to several factors, including climate, lithology-related erosion efficiency, and paleotopography. Models with more sophisticated forcing conditions may make it possible to better reconstruct the surface dynamics of Cretaceous Southern Africa.

5. Discussion

Offshore depositional histories can be used to reconstruct upstream erosion in a source-to-sink context (Hampson et al., 2014; Helland-Hansen et al., 2009; Tinker et al., 2008a) and to constrain the tectonic history (Calvès et al., 2018; Clift et al., 2006; Pechlivanidou et al., 2018). Enhanced sediment flux often corresponds to increased inland incision which can be related to upstream uplift (Baby et al., 2019; Braun et al., 2013, 2014; Ruetenik et al., 2016). Our Case 3 predicts an increase in the average offshore sedimentation rate during uplift of the central plateau between 10 and 20 Myr (Figure 1h). However, Case 3 also suggests that local offshore sedimentation can be affected by complex drainage reorganizations, blurring the tectonic history of the sediment source. For example, the increased sediment flux to the South Basin from 7 to 9 Myr (Figure 3b)

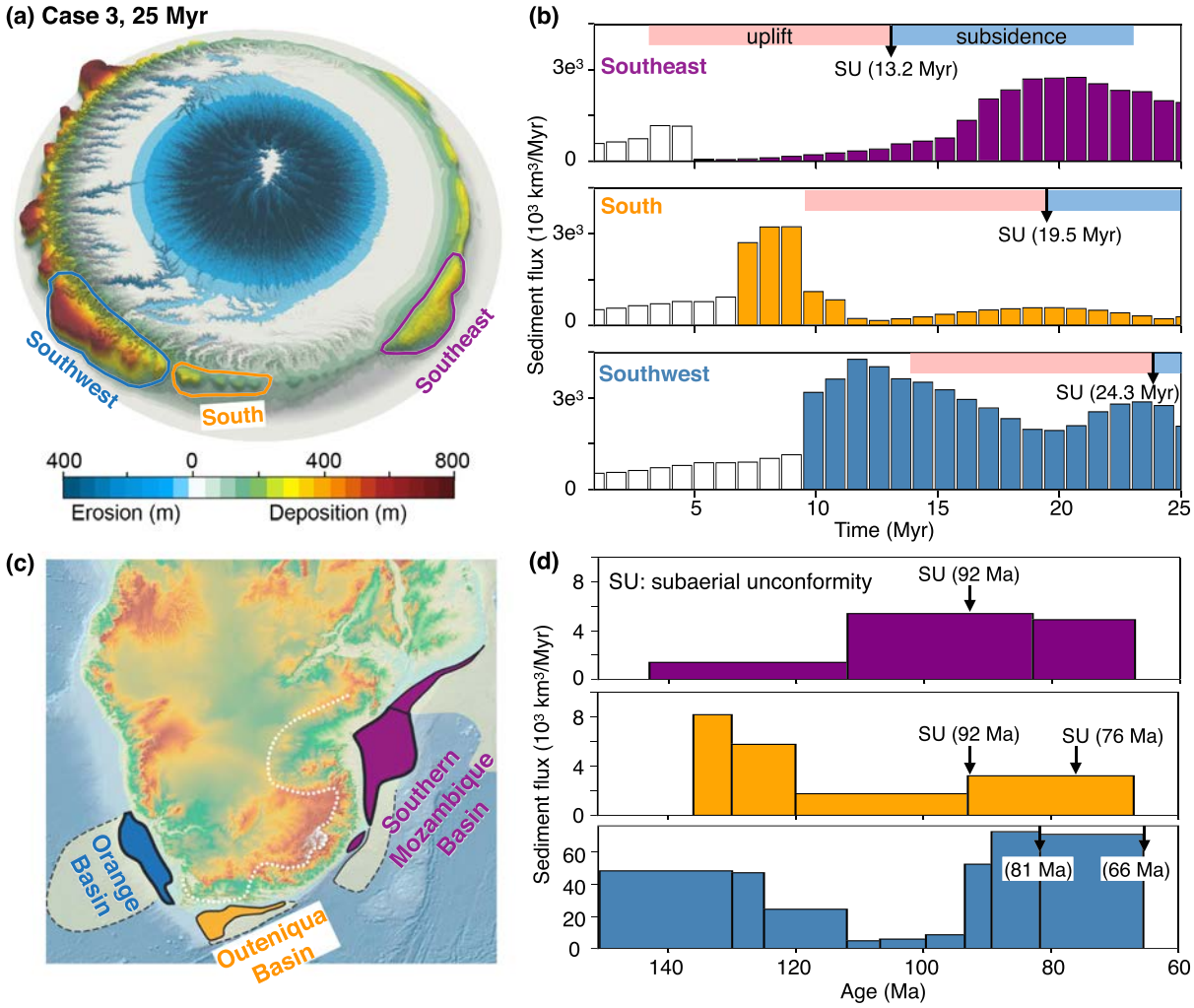

Figure 3. (a) Cumulative erosion and deposition for Case 3 at 25 Myr. Three marginal basins are considered: The Southeast, South, and Southwest Basins. (b) Sediment flux to the three basins from 0 to 25 Myr. The red and blue boxes show the time period during which the domain experiences uplift and subsidence. The timing of the subaerial unconformity (SU) formed at each basin is also indicated. (c) Offshore basins of Southern Africa (modified from Braun et al., 2014). (d) Sediment flux to the Southern Mozambique, Outeniqua, and Orange Basins across the Cretaceous Period (Guillocheau et al., 2012; Said et al., 2015; Tinker et al., 2008b). The timing of the subaerial unconformity (SU) is indicated for each basin.

is sourced from rerouted rivers from the eastern domain and is not associated with the uplift of the central plateau (Figure 1b). Counterintuitively, we also find that a reduced sediment flux can be induced by an uplift event. Indeed, the negligible sediment flux to the Southeast Basin from 5 to 10 Myr (Figure 3b) is related to margin uplift (Figure 1b).

The distinct stratal architectures along the margin in Case 3 are related to the relationship between the direction of propagation of the dynamic topography and the direction of sediment transport (Figure 3). To better understand those potential correlations, we pick nine offshore deltas along the margin (Figure S2) and reconstruct their sediment flux histories as well as stratal stacking patterns, based on which we summarize three types of sedimentary responses to a migrating dynamic topography (Figure 4). From Types 1 to 3, the direction of the migrating dynamic topography and that of sediment transport are opposite, perpendicular, and parallel respectively. In Type 1, sediment flux is negligible during dynamic uplift but significantly increases during dynamic subsidence. In Type 2, sediment flux is enhanced before dynamic uplift, it notably decreases during dynamic uplift and slightly increases during dynamic subsidence. In Type 3, sediment flux reveals a notable increase before the dynamic uplift phase. However, it remains large during dynamic uplift and decreases during the dynamic subsidence phase.

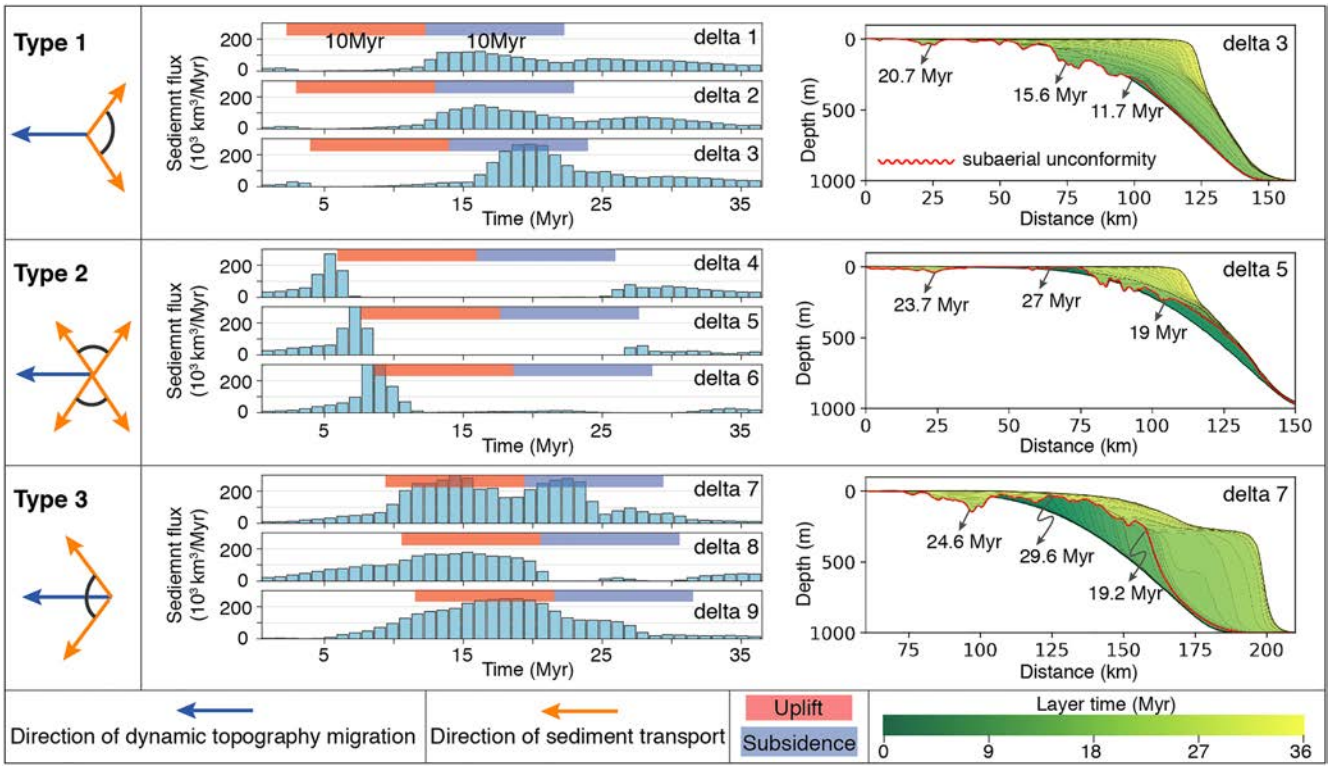

Figure 4. Three types of sedimentary responses to a migrating dynamic topography, depending on the angular relationship between the direction of dynamic topography migration and the direction of sediment transport. Nine individual deltas are picked (see locations in Figure S2 in the supporting information). Sediment flux histories are reconstructed for each delta. The time frames of the dynamic uplift and subsidence experienced by each delta are also indicated. Stratal stacking patterns are built up along dip-oriented profiles extracted at deltas 3, 5, and 7, respectively. The timing of the subaerial unconformity (red curve) is indicated for each stratal stacking pattern.

The stratal stacking patterns extracted at deltas 3, 5, and 7 share a common feature which is the formation of subaerial unconformities. Those unconformities are diachronous along the margin, as the sediment supply history driven by the laterally migrating dynamic topography is diachronous. This suggests that variations in sediment supply play a significant role (even a dominant role at delta 5) in controlling the formation of unconformities, supporting the supply-dominated sequences (Zhang et al., 2019). Our results can also provide important insights into identifying those supply-dominated sequences in outcrop and in the subsurface.

We further find that the duration of the depositional hiatus mirrors the duration of the dynamic uplift or subsidence (10 Myr in Case 3; Figure 4). The difference in the timing of the depositional hiatus for different deltas reflects the migration velocity (distance between two deltas divided by the difference in the initial time of the sedimentation gap) of the dynamic uplift. This suggests that series of erosional or depositional events could be correlated to identify the propagation of past dynamic uplift events.

Although dynamic topography is best identified for wavelengths greater than 2,500 km (Davies et al., 2019), wavelengths as short as ~300 km have been proposed (Hartley et al., 2011; Rudge et al., 2008). These short wavelengths interact with isostatic and flexural topography (e.g., McKenzie, 2010). We thus consider in Case 4 a wavelength of dynamic topography reduced to 300 km. This dynamic topography results in a cycle of 300 m uplift in 3 Myr and 300 m subsidence in the following 3 Myr. Its average rate of change (100 m/Myr) is comparable to the uplift of the northwest coast of Europe by >550 m in 2–3 Myr (Hartley et al., 2011). Our results show that although the propagating dynamic topography also induces river rerouting (Figures S3a–S3c), the drainage reorganizations do not last long enough to affect the erosion and deposition patterns, illustrating the response time of landscapes to external forcing. In contrast to Case 3, the central plateau in Case 4 is symmetrically eroded (Figures S3a–S3d), and offshore basins are of comparable sizes (Figure S3d). The effects of dynamic topography on marginal stratal stacking patterns and sediment supply histories are also less pronounced in Case 4 (Figures S3e and S3f) compared to Case 3.

6. Conclusions

We present a series of generic source-to-sink models to investigate the impact of dynamic topography on landscape evolution and stratigraphic formations. We show that source-to-sink systems respond differently to a migrating wave of dynamic topography and sea level fluctuations. Contrary to sea level variations, dynamic topography induces significant reorganizations of river networks and drives complex erosion and sediment routing responses in the source region. Variations in sediment supply, depending on the relative directions between dynamic topography propagation and sediment transport, contribute to the formation of diachronous unconformities along the margin. Long-wavelength dynamic topography (e.g., 1,000 km) has a greater impact on drainage reorganizations and sedimentary architectures than short-wavelength dynamic topography (e.g., 300 km). Correlating similar offshore depositional events has the potential to constrain the evolution of past dynamic topography. Our model also predicts, to the first order, the sediment flux histories along the southern African margins during Cretaceous times. We finally show that source-to-sink modeling approach provides an efficient and powerful tool to explore the interplay between dynamic topography and surface processes. It can help decipher the geomorphic and stratigraphic signals of dynamic topography in the geological record.

Acknowledgments

X. D., T. S., C. M., and P. R. were supported by ARC grant IH130200012, and N. F. was supported by ARC grant DE160101020. This research was undertaken with the assistance of resources and services from the National Computational Infrastructure, which is supported by the Australian Government. We thank Peter Burgess and an anonymous reviewer for their constructive comments on this paper. The code, inputs, and post-processing functions used in this study are available online at https://github.com/XuesongDing/DynTopo_Stratigraphy_LEM website.

References

Baby, G., Guillocheau, F., Boulogne, C., Robin, C., & Dall'Asta, M. (2018). Uplift history of a transform continental margin revealed by the stratigraphic record: The case of the Agulhas transform margin along the Southern African Plateau. *Tectonophysics*, *731*, 104–130.

Baby, G., Guillocheau, F., Braun, J., Robin, C., & Dall'Asta, M. (2019). Solid sedimentation rates history of the Southern African continental margins: Implications for the uplift history of the South African Plateau. *Terra Nova*, ter.12435. https://doi.org/10.1111/ter.12435

Baby, G., Guillocheau, F., Morin, J., Ressouche, J., Robin, C., Broucke, O., & Dall'Asta, M. (2018). Post-rift stratigraphic evolution of the Atlantic margin of Namibia and South Africa: Implications for the vertical movements of the margin and the uplift history of the South African Plateau. *Marine and Petroleum Geology*, *97*, 169–191.

Bijwaard, H., & Spakman, W. (1999). Tomographic evidence for a narrow whole mantle plume below Iceland. *Earth and Planetary Science Letters*, *166*(3), 121–126.

Braun, J. (2010). The many surface expressions of mantle dynamics. *Nature Geoscience*, *3*(12), 825.

Braun, J., Guillocheau, F., Robin, C., Baby, G., & Jelsma, H. (2014). Rapid erosion of the Southern African Plateau as it climbs over a mantle superswell. *Journal of Geophysical Research: Solid Earth*, *119*, 6093–6112. https://doi.org/10.1002/2014JB010998

Braun, J., Robert, X., & Simon-Labric, T. (2013). Eroding dynamic topography. *Geophysical Research Letters*, *40*, 1494–1499. https://doi.org/10.1002/grl.50310

Brown, R. W., Summerfield, M. A., & Gleadow, A. J. W. (2002). Denudational history along a transect across the Drakensberg Escarpment of southern Africa derived from apatite fission track thermochronology. *Journal of Geophysical Research*, *107*(B12), 2350. https://doi.org/10.1029/2001JB000745

Burgess, P. M., Gurnis, M., & Moresi, L. (1997). Formation of sequences in the cratonic interior of North America by interaction between mantle, eustatic, and stratigraphic processes. *Geological Society of America Bulletin*, *109*(12), 1515–1535.

Burgess, P. M., & Moresi, L. (1999). Modelling rates and distribution of subsidence due to dynamic topography over subducting slabs: Is it possible to identify dynamic topography from ancient strata? *Basin Research*, *11*(4), 305–314.

Calvès, G., Calderón, Y., Hurtado Enriquez, C., Brusset, S., Santini, W., & Baby, P. (2018). Mass balance of Cenozoic Andes-Amazon source to sink system—Marañón Basin, Peru. *Geosciences*, *8*(5), 167.

Champion, M. E., White, N. J., Jones, S. M., & Lovell, J. P. B. (2008). Quantifying transient mantle convective uplift: An example from the Faroe-Shetland basin. *Tectonics*, *27*, TC1002. https://doi.org/10.1029/2007TC002106

Chang, C., & Liu, L. (2019). Distinct responses of intraplate sedimentation to different subsidence mechanisms: Insights from forward landscape evolution simulations. *Journal of Geophysical Research: Earth Surface*, *124*, 1139–1159. https://doi.org/10.1029/2018JF004905

Clift, P. D., Blusztajn, J., & Nguyen, A. D. (2006). Large-scale drainage capture and surface uplift in eastern Tibet-SW China before 24 Ma inferred from sediments of the Hanoi Basin, Vietnam. *Geophysical Research Letters*, *33*, L19403. https://doi.org/10.1029/2006GL027772

Czarnota, K., Hoggard, M. J., White, N., & Winterbourne, J. (2013). Spatial and temporal patterns of Cenozoic dynamic topography around Australia. *Geochemistry, Geophysics, Geosystems*, *14*, 634–658. https://doi.org/10.1029/2012GC004392

Czarnota, K., Roberts, G. G., White, N. J., & Fishwick, S. (2014). Spatial and temporal patterns of Australian dynamic topography from River Profile Modeling. *Journal of Geophysical Research: Solid Earth*, *119*, 1384–1424. https://doi.org/10.1002/2013JB010436

Davies, D. R., Valentine, A. P., Kramer, S. C., Rawlinson, N., Hoggard, M. J., Eakin, C. M., & Wilson, C. R. (2019). Earth's multi-scale topographic response to global mantle flow. *Nature Geoscience*, *12*(10), 845–850. https://doi.org/10.1038/s41561-019-0441-4

Ding, X., Salles, T., Flament, N., & Rey, P. (2019). Quantitative stratigraphic analysis in a source-to-sink numerical framework. *Geoscientific Model Development*, *12*(6), 2571–2585. https://doi.org/10.5194/gmd-12-2571-2019

Downey, N. J., & Gurnis, M. (2009). Instantaneous dynamics of the cratonic Congo basin. *Journal of Geophysical Research*, *114*, B06401. https://doi.org/10.1029/2008JB006066

Eakin, C. M., & Lithgow-Bertelloni, C. (2018). An overview of dynamic topography: The influence of mantle circulation on surface topography and landscape. *Mountains, Climate and Biodiversity*, *37*.

Flament, N., Gurnis, M., & Müller, R. D. (2013). A review of observations and models of dynamic topography. *Lithosphere*, *5*(2), 189–210.

Flament, N., Gurnis, M., Williams, S., Seton, M., Skogseid, J., Heine, C., & Müller, R. D. (2014). Topographic asymmetry of the South Atlantic from global models of mantle flow and lithospheric stretching. *Earth and Planetary Science Letters*, *387*, 107–119.

Guillocheau, F., Rouby, D., Robin, C., Helm, C., & Rolland, N. (2012). Quantification and causes of the terrigenous sediment budget at the scale of a continental margin: A new method applied to the Namibia-South Africa margin. *Basin Research*, *24*(1), 3–30.

Gurnis, M., Mitrovica, J. X., Ritsema, J., & van Heijst, H. (2000). Constraining mantle density structure using geological evidence of surface uplift rates: The case of the African superplume. *Geochemistry, Geophysics, Geosystems*, *1*(7). https://doi.org/10.1029/1999GC000035

Hampson, G. J., Duller, R. A., Petter, A. L., Robinson, R. A. J., & Allen, P. A. (2014). Mass-balance constraints on stratigraphic interpretation of linked alluvial-coastal-shelfal deposits from source to sink: Example from Cretaceous Western Interior Basin, Utah and Colorado, USA. *Journal of Sedimentary Research*, *84*(11), 935–960.

Hartley, R. A., Roberts, G. G., White, N., & Richardson, C. (2011). Transient convective uplift of an ancient buried landscape. *Nature Geoscience*, *4*(8), 562.

Helland-Hansen, W., Martinsen, O. J., & Thurmond, J. B. (2009). Relationships between morphological and sedimentological parameters in source-to-sink systems: A basis for predicting semi-quantitative characteristics in subsurface systems. *Basin Research*, *21*(4), 361–387.

Hu, J., Liu, L., Faccenda, M., Zhou, Q., Fischer, K. M., Marshak, S., & Lundstrom, C. (2018). Modification of the Western Gondwana craton by plume-lithosphere interaction. *Nature Geoscience*, *11*(3), 203.

Hunt, D., & Tucker, M. E. (1992). Stranded parasequences and the forced regressive wedge systems tract: Deposition during base-level fall. *Sedimentary Geology*, *81*(1–2), 1–9.

Karlstrom, K. E., Coblentz, D., Dueker, K., Ouimet, W., Kirby, E., Van Wijk, J., et al., & CREST Working Group (2012). Mantle-driven dynamic uplift of the Rocky Mountains and Colorado Plateau and its surface response: Toward a unified hypothesis. *Lithosphere*, *4*(1), 3–22. https://doi.org/10.1130/L150.1

Liu, L., & Gurnis, M. (2010). Dynamic subsidence and uplift of the Colorado Plateau. *Geology*, *38*(7), 663–666.

Maclennan, J., McKenzie, D., & Gronvöld, K. (2001). Plume-driven upwelling under central Iceland. *Earth and Planetary Science Letters*, *194*(1), 67–82.

Matthews, K. J., Hale, A. J., Gurnis, M., Müller, R. D., & DiCaprio, L. (2011). Dynamic subsidence of Eastern Australia during the Cretaceous. *Gondwana Research*, *19*(2), 372–383.

McKenzie, D. (2010). The influence of dynamically supported topography on estimates of Te. *Earth and Planetary Science Letters*, *295*(1–2), 127–138. https://doi.org/10.1016/J.EPSL.2010.03.033

Miller, K. G., Kominz, M. A., Browning, J. V., Wright, J. D., Mountain, G. S., Katz, M. E., et al. (2005). The Phanerozoic record of global sea-level change. *Science*, *310*(5752), 1293–1298. https://doi.org/10.1126/science.1116412

Moucha, R., & Forte, A. M. (2011). Changes in African topography driven by mantle convection. *Nature Geoscience*, *4*(10), 707.

Moucha, R., Forte, A. M., Rowley, D. B., Mitrovica, J. X., Simmons, N. A., & Grand, S. P. (2009). Deep mantle forces and the uplift of the Colorado Plateau. *Geophysical Research Letters*, *36*, L19310. https://doi.org/10.1029/2009GL039778

Neal, J., & Abreu, V. (2009). Sequence stratigraphy hierarchy and the accommodation succession method. *Geology*, *37*(9), 779–782.

Neal, J., Abreu, V., Bohacs, K. M., Feldman, H. R., & Pederson, K. H. (2016). Accommodation succession (δA/δS) sequence stratigraphy: observational method, utility and insights into sequence boundary formation. *Journal of the Geological Society*, *173*(5), 803–816.

Pechlivanidou, S., Cowie, P. A., Hannisdal, B., Whittaker, A. C., Gawthorpe, R. L., Pennos, C., & Riiser, O. S. (2018). Source-to-sink analysis in an active extensional setting: Holocene erosion and deposition in the Sperchios rift, central Greece. *Basin Research*, *30*(3), 522–543.

Rudge, J. F., Shaw Champion, M. E., White, N., McKenzie, D., & Lovell, B. (2008). A plume model of transient diachronous uplift at the Earth's surface. *Earth and Planetary Science Letters*, *267*(1–2), 146–160. https://doi.org/10.1016/J.EPSL.2007.11.040

Ruetenik, G. A., Moucha, R., & Hoke, G. D. (2016). Landscape response to changes in dynamic topography. *Terra Nova*, *28*(4), 289–296.

Said, A., Moder, C., Clark, S., & Ghorbal, B. (2015). Cretaceous-Cenozoic sedimentary budgets of the Southern Mozambique Basin: Implications for uplift history of the South African Plateau. *Journal of African Earth Sciences*, *109*, 1–10.

Salles, T., Ding, X., & Brocard, G. (2018). pyBadlands: A framework to simulate sediment transport, landscape dynamics and basin stratigraphic evolution through space and time. *PLoS ONE*, *13*(4), e0195557.

Salles, T., Flament, N., & Müller, D. (2017). Influence of mantle flow on the drainage of eastern Australia since the Jurassic Period. *Geochemistry, Geophysics, Geosystems*, *18*, 280–305. https://doi.org/10.1002/2016GC006617

Salles, T., & Hardiman, L. (2016). Badlands: An open-source, flexible and parallel framework to study landscape dynamics. *Computers & Geosciences*, *91*, 77–89.

Sandiford, M. (2007). The tilting continent: A new constraint on the dynamic topographic field from Australia. *Earth and Planetary Science Letters*, *261*(1–2), 152–163.

Stanley, J. R., Flowers, R. M., & Bell, D. R. (2015). Erosion patterns and mantle sources of topographic change across the southern African Plateau derived from the shallow and deep records of kimberlites. *Geochemistry, Geophysics, Geosystems*, *16*, 3235–3256. https://doi.org/10.1002/2015GC005969

Tinker, J., de Wit, M., & Brown, R. (2008a). Linking source and sink: Evaluating the balance between onshore erosion and offshore sediment accumulation since Gondwana break-up, South Africa. *Tectonophysics*, *455*(1–4), 94–103.

Tinker, J., de Wit, M., & Brown, R. (2008b). Mesozoic exhumation of the southern Cape, South Africa, quantified using apatite fission track thermochronology. *Tectonophysics*, *455*(1–4), 77–93.

Vail, P. R., Mitchum, J. R. M., & Thompson, S. III (1977). Seismic strat igraphy and global changes of sea level: Part 4. Global cycles of relative changes of sea level. In C. E. Payton (Ed.). *Seismic stratigraphy application to hydrocarbon exploration: American Association of Petroleum Geologists Memoir* (Vol. 26, pp. 205–212).

Zhang, J., Burgess, P. M., Granjeon, D., & Steel, R. (2019). Can sediment supply variations create sequences? Insights from stratigraphic forward modelling. *Basin Research*, *31*(2), 274–289.

References From the Supporting Information

Avouac, J.-P., & Burov, E. B. (1996). Erosion as a driving mechanism of intracontinental mountain growth. *Journal of Geophysical Research*, *101*(B8), 17747–17769.

Chen, A., Darbon, J., & Morel, J.-M. (2014). Landscape evolution models: A review of their fundamental equations. *Geomorphology*, *219*, 68–86.

Flemings, P. B., & Jordan, T. E. (1989). A synthetic stratigraphic model of foreland basin development. *Journal of Geophysical Research*, *94*(B4), 3851–3866.

Granjeon, D., & Joseph, P. (1999). Concepts and applications of a 3-D multiple lithology, diffusive model in stratigraphic modeling.

Meijer, X. D. (2002). Modelling the drainage evolution of a river-shelf system forced by Quaternary glacio-eustasy. *Basin Research*, *14*(3), 361–377.

Paola, C., Heller, P. L., & Angevine, C. L. (1992). The large-scale dynamics of grain-size variation in alluvial basins, 1: Theory. *Basin Research*, *4*(2), 73–90.

SEPM Strata, http://www.sepmstrata.org/Terminology.aspx?id = Wheeler%20diagram (accessed 30 October, 2019).